Proceedings of the XVII ECSMGE-2019
Geotechnical Engineering foundation of the future
ISBN 978-9935-9436-1-3

doi: 10.32075/17ECSMGE-2019-0461

XVII European Conference
ECSMGE 2019
Reykjavik
on Soil Mechanics
and Geotechnical Engineering

Numerical simulation of swelling soil – mat foundation interaction

Simulation numérique de l'interaction entre sol gonflant et radier

D. Loukidis
University of Cyprus, Nicosia, Cyprus

G. Lazarou
University of Cyprus, Nicosia, Cyprus

M. Bardanis
Edafos Engineering Consultants S.A., Athens, Greece

ABSTRACT: Volume changes exhibited by expansive soils upon wetting and drying are responsible for various degrees of damage to buildings. This paper presents a simple constitutive model intended for use in finite element analyses of the interaction between mat foundations and expansive soils subjected to changes in moisture content. The constitutive model combines a nonlinear elastic law with a mechanism that predicts plastic volumetric strains caused by changes in soil suction. The model has been implemented in a finite element program and calibrated against experimental data from swelling/collapse oedometer tests on an expansive Nicosia marl. Coupled mechanical-unsaturated flow finite element simulations are performed for circular and strip mats resting on Nicosia marl, using daily climatic input, namely rainfall and evaporation, consistent with the semi-arid climate of Nicosia, Cyprus, for the course of seventeen months. Analyses show that soil volume changes caused by moisture migration in the vicinity of the foundation can generate significant bending moments, especially during the dry season.

RÉSUMÉ: Les changements de volume présentés par les sols expansifs lors du mouillage et du séchage sont responsables de divers degrés de dommages aux bâtiments. Cet article présente un modèle constitutif simple destiné à être utilisé dans l'analyse des éléments finis de l'interaction entre radiers et sols expansifs. Le modèle constitutif combine une loi élastique avec un mécanisme qui conduit au développement des contraintes volumétriques plastique causées par des modifications de la succion du sol. Le modèle a été mis en œuvre dans un programme d'éléments finis et calibré sur des données expérimentales issues d'essais d'œdomètre de gonflement/effondrement sur une marne de Nicosie expansive. Des simulations couplés par éléments finis (mécanique - flux insaturé) sont effectuées pour radiers circulaires et de bande reposants sur la marne de Nicosie, en utilisant les données climatiques quotidiennes (précipitation et évaporation) compatibles avec le climat semi-aride de Nicosie, Chypre, pendant une période de dix-sept mois. Les analyses montrent que les changements de volume du sol dus à la migration de l'humidité à proximité de la fondation peuvent générer des moments de flexion significatifs, en particulier pendant la saison sèche.

Keywords: Numerical simulation; Swelling soil; Mat foundation; Coupled analysis; Volumetric strains

1 INTRODUCTION

Expansive soils are responsible for various degrees of damage to structures, with an annual cost of the order of billions of dollars worldwide. Such soils cover large areas of the island of Cyprus, especially in the Mesaoria basin, where the city of Nicosia is located. Moreover, Cyprus' climate is characterized by hot and dry summers and rainy winters, aggravating the impact of the soil swelling/shrinkage to buildings supported by shallow foundations. The frequency and severity of such damages is still very high, indicating the need to implement reliable methods for the analysis and design of shallow foundations that would take into account the actions to the foundation elements caused by soil swelling/shrinkage.

The study of the interaction between expansive soils and foundations is a prerequisite for the development of design methods for mat foundations on expansive soils, such as those by Walsh (1974), Wray (1989), Poulos (1984). Coupled flow-mechanical finite element analysis has been employed by several researchers in order to study both the migration of moisture under a foundation slab and the effects of the resulting differential heave and settlement. In most of these studies, the soil is assumed to be elastic, with the added ability to develop additional volumetric strains upon changes in matric suction (e.g. Li et al. 1995; Vu & Fredlund 2004). More recently, Jahangir et al. (2012) performed finite element analyses in which the advanced elastoplastic constitutive model of Alonso et al. (1999) was used.

This paper presents a simple constitutive model meant to be used in finite element analyses of mat foundation – expansive soil interaction for the determination of the flexure and bending moments caused by ground moisture changes. The model follows a nonlinear elastic law combined with a mechanism for the development of inelastic volumetric strains upon changes in soil suction and is calibrated for a medium to highly expansive Nicosia marl. Coupled mechanical – unsaturated flow finite element simulations of mat – soil interaction are performed in order to demonstrate the capabilities of the model and shed light on the impact of climate-induced soil swelling/shrinkage to the bending of mat foundations.

2 EXPERIMENTAL DATA

Nicosia brown (or khaki) marl is a highly calcareous stiff silty clay ($CaCO_3$ of the order of 30%-50%) deposited in a marine environment during the Pliocene. Its expansiveness is due to a montmorillonite content that falls often in the 10% to 20% range (Constantinou et al. 2002). Marl samples were collected in summer (dry season) from a 1.5m deep test pit at a location in the University of Cyprus campus where the marl is outcropping. Care was taken to prevent loss of moisture during transportation and storage.

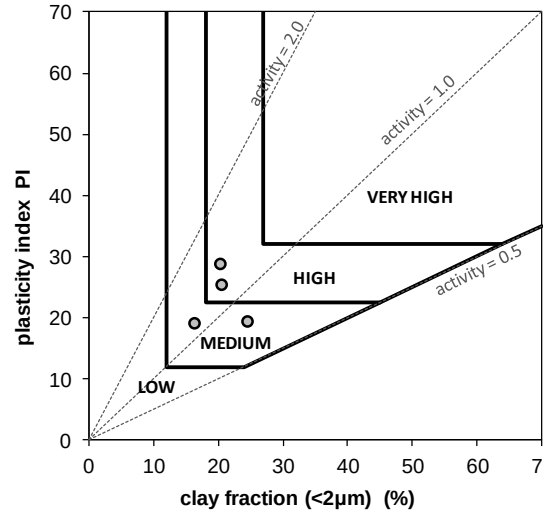

Figure 1. Potential expansiveness of sampled Nicosia marl according to the South African chart.

The index properties and classification of the sampled marl are summarized in Table 1. The plasticity index (PI) ranges from 19 to 29 and the clay content from 16% to 25%. Based on this, the marl is characterized according to the

Table 1. Index properties and classification of marl samples.

Sample	clay (%)	silt (%)	LL	PI	γ_d (kN/m^3)	USCS
1	20	62	54	29	15.2	CH
2	21	63	52	25	15.9	CH
3	25	63	45	19	15.8	CL
4	16	62	39	19	15.8	CL

South African chart (van der Merwe 1975; Williams and Donaldson 1980) as potentially medium to marginally highly expansive (Fig. 1).

The soil-water characteristic curve (SWCC) was determined in terms of total suction (i.e. matric suction plus osmotic suction) using a WP4C chilled mirror hygrometer (Decagon Inc.). Measurements were made for samples at their natural (as sampled) moisture content, as well as on wetted and dried samples (Fig. 2). At their natural water content, ranging from 10% to 14% (degree of saturation 39% to 57%), the corresponding total suction is 5.70MPa to 8.75MPa.

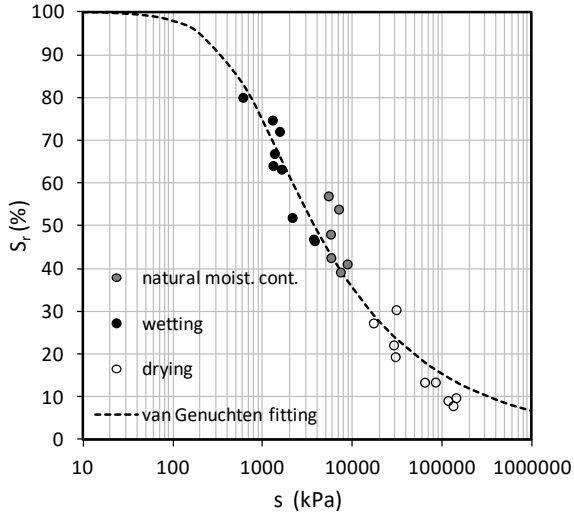

Figure 2. Soil-water characteristic curve.

The data in Fig. 2 were fitted using the van Genuchten equation (van Genuchten 1980; Galavi 2010):

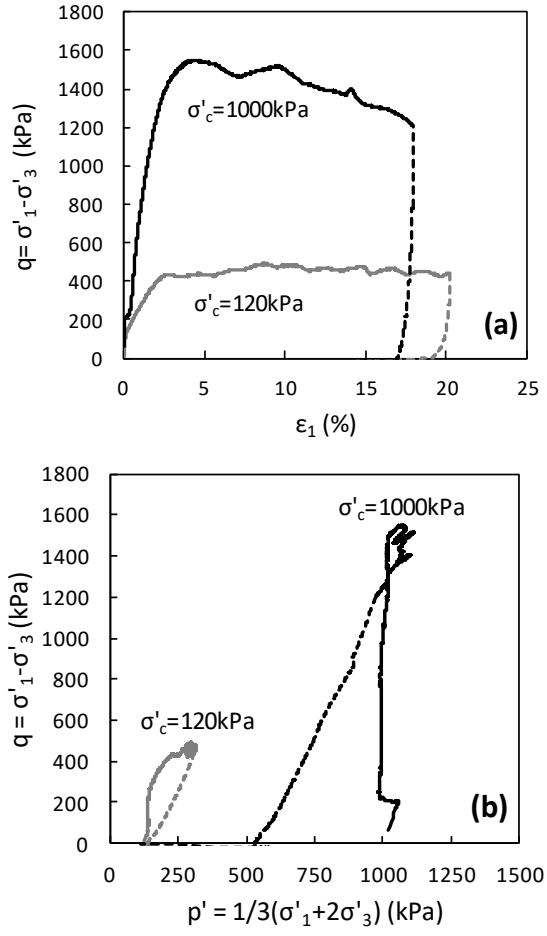

Figure 3. CU triaxial tests: a) stress-strain curves, b) effective stress paths.

$$S_r(s) = S_{r,res} + \left(1 - S_{r,res}\right)\left[1 + \left(g_a \left|\frac{s}{\gamma_w}\right|\right)^{g_n}\right]^{g_c} \quad (1)$$

where S_r is the degree of saturation, s is the soil suction, γ_w is the water unit weight, $S_{r,res}$ is the residual degree of saturation, while g_a, g_n and g_c are fitting parameters. Nonlinear fitting using Excel solver resulted in g_a = 0.016, g_n = 1.37 and $S_{r,res}$ = 0, while g_c was set equal to $(1-g_n)/g_n$ following Mualem (1976).

Fig. 3 shows the results from CU triaxial tests at two initial effective confining pressures σ_c'. The dashed lines in the plots correspond to unloading. Given that the elastic part of the constitutive model is formulated based on Hooke's law, the triaxial tests are used here for the determination of the Young's modulus E, which at deviatoric stress 50% of the peak is 29.4MPa and 74.2MPa for σ_c' equal to 120kPa and 1000kPa, respectively.

The swelling/collapse behavior of the Nicosia marl was studied in oedometer tests (Fig. 4). In these tests, undisturbed samples were initially subjected to various vertical loads, ranging from 4kPa to 250kPa, at their natural water content. Subsequently, the specimens were inundated with deionised water to full saturation while measuring the resulting volumetric strains.

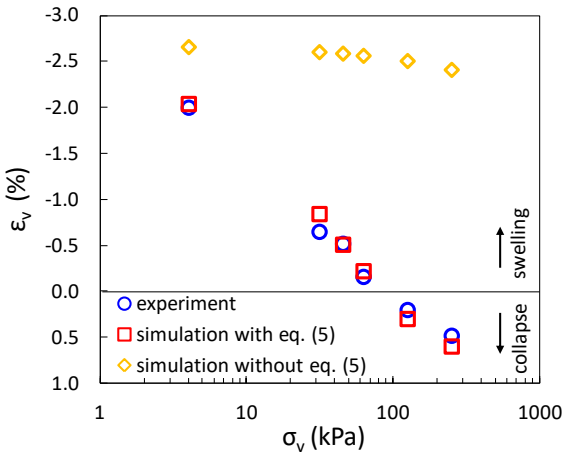

Figure 4. Volumetric strain due to inundation at various values of overburden stress: experimental data vs. model predictions.

In Fig. 4, it can be seen that under "free swelling" conditions (σ_v=4kPa) the final vertical strain is 2%, while collapse occurred for σ_v larger than 90kPa.

3 CONSTITUTIVE MODEL

3.1 Model formulation

The constitutive model makes use of the Bishop's effective stress definition in the form that exists in the software Plaxis (Galavi, 2010) assuming constant air pressure:

$$\dot{\sigma}'_{ij} = \dot{\sigma}_{ij} - (\chi u_w)\delta_{ij} \tag{2}$$

where σ'_{ij} and σ_{ij} are the effective and total stress tensors, δ_{ij} is the Kronecker delta, u_w is the pore water pressure and χ is the effective stress parameter, which is taken herein equal to the degree of saturation S_r. For partially saturated soil, u_w=-s.

The elastic part of the model formulation follows the Hooke's law:

$$\dot{\sigma}'_{ij} = D_{ijkl}\dot{\varepsilon}_{el,kl} \tag{3}$$

where $\varepsilon_{el,ij}$ is the elastic strain tensor and D_{ijkl} is the isotropic elastic stiffness matrix defined in terms of Young's modulus E and Poisson's ratio v. The modulus E is set to depend on the effective vertical stress σ_v' according to a power law:

$$E = A\sigma_v'^{\,n} p_a^{\,1-n} \tag{4}$$

where p_a=100kPa and σ_v' is the vertical effective stress.

In order to be able to reproduce collapse upon inundation, as well as the correct swelling behavior of the soil, the model is made to predict inelastic volumetric strains upon changes of suction using the following equation:

$$\dot{\varepsilon}_{vpl} = -\frac{a\dot{s}\chi - (1-a)\langle -\dot{s}\rangle\chi}{D_{vpl}} \tag{5}$$

where a is a model parameter and $< \cdot >$ are the Macaulay brackets. Eq.(5) predicts positive (contractive) plastic strain when suction decreases, while negative (expansive) plastic strain is generated when suction increases, but at a different rate as a consequence of the parameter a and the Macaulay brackets. The latter is instrumental for preventing the model from predicting volume expansion during drying. D_{vpl} is a plastic modulus given by

$$D_{\mathrm{vpl}} = p_{\mathrm{a}} / 3 + B\sigma_{\mathrm{v}}'^{m} p_{\mathrm{a}}^{1-m} \tag{6}$$

The factor B is set to be a decreasing function of the vertical total stress σ_{v} according to equation

$$B = \frac{c_1}{1 + c_3(\sigma_{\mathrm{v}} / p_{\mathrm{a}})} + c_2 \tag{7}$$

In eqs. (4)-(7), the A, n, m, α, c_1, c_2, c_3 are model parameters.

The plastic volumetric strain is apportioned equally among the three normal strains, i.e. $\dot{\varepsilon}_{\mathrm{pl},ij} = \dot{\varepsilon}_{\mathrm{vpl}} / 3$ for $i=j$, while $\dot{\varepsilon}_{\mathrm{pl},ij} = 0$ for $i \neq j$. Elastic and plastic strains are superimposed to yield the total strains ε_{ij}

$$\dot{\varepsilon}_{ij} = \dot{\varepsilon}_{\mathrm{el},ij} + \dot{\varepsilon}_{\mathrm{pl},ij} \tag{8}$$

and the elastic stress-strain law of eq. (3) can be rewritten as

$$\dot{\sigma}'_{ij} = D_{ijkl}(\dot{\varepsilon}_{ij} - \dot{\varepsilon}_{\mathrm{pl},ij}) \tag{9}$$

3.2 Model calibration

Table 2 presents the model parameters entering eqs. (4)-(7). The parameters A and n are determined from the triaxial tests (Fig. 3), while the Poisson's ratio v was assumed to be equal to 0.25. The parameters m, c_1, c_2 and c_3 are determined from coupled finite element simulations of the inundation tests in oedometer of Fig. 4 via a trial and error procedure, assuming all the samples having an initial S_{r} equal to 52%. The model was implemented in the finite element program Plaxis 2D via a user subroutine written in Fortran.

In a finite element computations environment, the user subroutine is called to update the effective stresses at each Gauss quadrature point using as input the total strain and suction rates produced by the global solution algorithm of the finite element analysis (solution of nodal force equilibrium and flow equations). During wetting, the plastic strains are positive, resulting in an additional decrease in the effective stresses (eq. 9). This generates compressive unbalanced forces, which in the next global solution equilibrium iteration will produce extra strains that will be contractive. These extra strains become larger with increasing σ_{v} (eq. 7), resulting in collapse response for σ_{v} >90kPa for the given marl.

Fig. 4 compares the simulation predictions to the experimental data from the oedometer swelling/collapse tests. It can be seen that the model is able to predict the observed contraction during wetting at overburden stress σ_{v} equal to 125kPa and 250kPa. If eq. (5) is ignored ($\varepsilon_{\mathrm{vpl}}$=0), the model would predict only swelling behavior, largely independent of the overburden stress. Herein, the parameter a was selected such that the strain developing during wetting at low overburden stress σ_{v} is recovered during subsequent drying back to the initial state.

Table 2. Constitutive model parameters for hard brown Nicosia marl.

Symbol	Value
A	394
n	0.2
v	0.25
m	0.4
a	0.75
c_1	1360
c_2	146
c_3	19.2

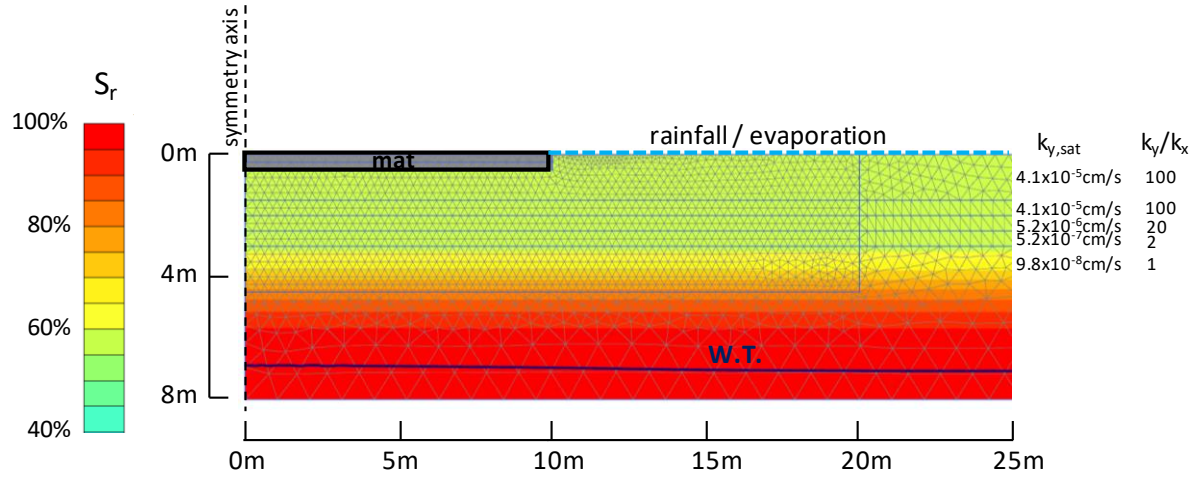

Figure 5. Profile of hydraulic properties and initial degree of saturation considered in FE analyses.

4 MAT-SOIL INTERACTION SIMULATIONS

4.1 Finite element model

Plaxis 2D is used for performing coupled simulations of the interaction of a circular mat (axisymmetric problem) using the above constitutive model with the parameters of Table 2. The mat has a diameter of 20m and thickness 0.5m, and it is loaded by a uniform load of either 12kPa or 24kPa, roughly corresponding to the equivalent loading of a one-storey and a two-storey building, respectively. For comparison purposes, analyses are performed also for the case of a very elongated mat (strip) of 20m width and same thickness, under plane strain conditions. The adopted soil profile is that of a location in the University of Cyprus campus where Nicosia marl is outcropping. The water table is at around 7m depth and exhibits minimal fluctuations in the duration of a hydrological year.

The unsaturated flow in Plaxis is modeled following Darcy's law, in which the permeability is a function of the soil suction s according to the following equation (van Genuchten 1980, Galavi 2010):

$$k(s) = k_{sat}\left(\frac{S_r(s)-S_{r,res}}{1-S_{r,res}}\right)^{g_l} \times \left[1-\left(1-\left(\frac{S_r(s)-S_{r,res}}{1-S_{r,res}}\right)^{-\frac{1}{g_c}}\right)^{-g_c}\right]^2 \quad (10)$$

where k_{sat} is the hydraulic conductivity of the soil when fully saturated. The exponent g_l is a model parameter that controls the rate of reduction of k with decreasing S_r. Herein, g_l is set equal to -5, yielding hydraulic conductivity two orders of magnitude smaller than k_{sat} for S_r in the range 55%-60%.

The simulated ground includes a desiccated crust about 3m thick. Fig. 5 shows contours of the initial degree of saturation, along with the assumed values of apparent in-situ hydraulic conductivity k_{sat}. The latter were established via back-calculation of a field wetting experiment at a site instrumented with suction and water content sensors (Lazarou et al. 2019). Anisotropy is considered in the hydraulic conductivity, with the vertical permeability being generally higher than the horizontal, especially in the upper portion of the profile, which is affected by desiccation cracking.

In the simulations, the ground surface not occupied by the mat is subjected to rainfall (positive infiltration) and evaporation (negative infiltration) for a time span of 17 months, namely from May 2014 to September 2015. This period includes an above average rainy winter and two very dry summers. Rainfall data (Fig. 6) comes from a nearby weather station and evaporation is estimated based on pan evaporation data scaled down to balance annual evaporation from the ground with annual rainfall (Lazarou et al. 2019). This assumption is consistent with arid to semi-arid climates, such as that of Cyprus.

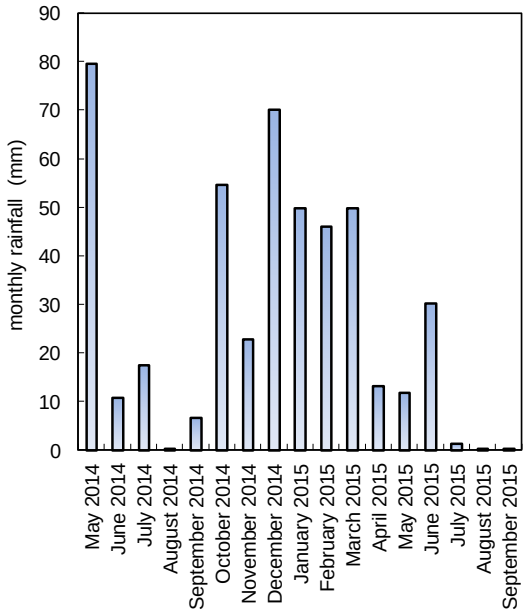

Figure 6. Rainfall data considered in FE simulations.

Both soil and mat are discretized using 15-noded triangular elements. The concrete material of the mat is assumed to behave always elastically with Young's modulus 32GPa, Poisson's ratio 0.2, and unit weight 25kN/m^3. The mat is assumed to be always in contact with the ground (no interface elements between mat and soil). In order to monitor the bending moments developing in the mat, a string of beam elements is placed in the middle of the mat cross-section (neutral axis). The stiffness of the beam elements is set to be 10^{-6} times the flexural stiffness of the mat, so that their presence has negligible influence in the mat deformation. The bending moments developing in the mat can be simply extracted by multiplying the bending moment diagram outputted for the beam elements by 10^6.

4.2 Numerical results

Fig. 7 shows the deformed mesh from the analysis of a circular mat loaded by 24kPa, at the last day of March 2015 and September 2015, i.e. at the end of the rainy and dry seasons, respectively. Deformations are exaggerated to different degrees in each case. It may be observed that, at the end of the rainy season, the soil has swelled, putting the slab in a slight "edge lift" mode (bottom fiber in tension).

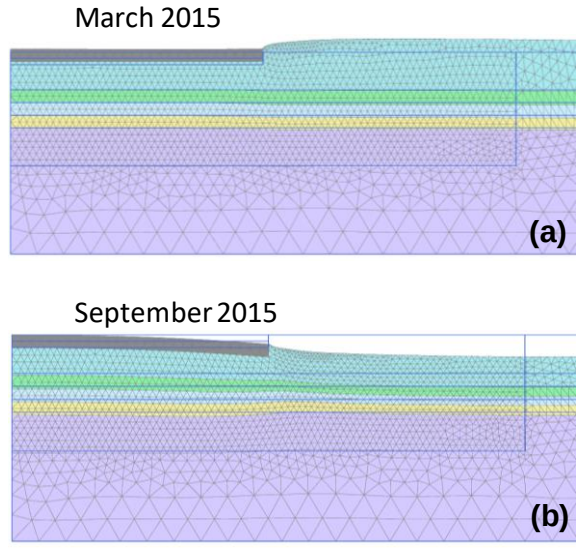

Figure 7. Examples of deformed mesh at the end of a) rainy season and b) dry season.

Contrarily, at the end of the dry season, the soil not covered by the mat and, thus, exposed to evaporation has shrunk relative to the soil under the mat, leading to a "center lift" deformation mode. In the particular case examined in this paper, there is an additional factor contributing

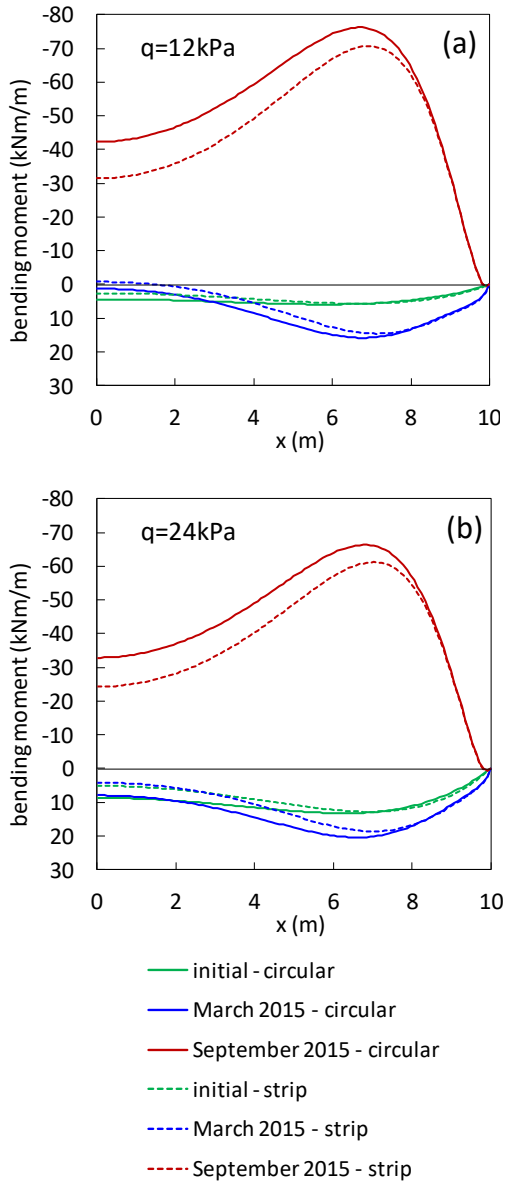

Figure 8. Bending moment diagrams along the mat.

to the development of center lift. This is the monotonic mid-term rise of moisture from the water table, which, unable to escape to the atmosphere due to the presence of the impermeable mat, it is accumulated under the mat central region (Lazarou et al. 2019).

The impact of these deformations to the stress state of the mat can be seen in Fig. 8, where the bending moments at three stages are plotted: i) after mat placement and loading, and before applying climatic input (initial state), ii) at the end of the rainy season (March 2015), and iii) at the end of the dry season (September 2015). In these plots, position x=0 corresponds to the center of the mat and x=10m to the mat edge. It can be seen that water infiltration during winter leads to an increase in the peak bending moment of the order of 50% in the case of the mat loaded by q=24kPa (Fig. 8b). On the other hand, when the mat loading is smaller (Fig. 8a), the increase is much larger (by a factor of 2.6). This is because the larger overburden stress suppresses the tendency of the soil under the mat edge to swell.

The case of center lift (September 2015) is by far the most critical, with the peak bending moments being almost one order of magnitude larger than those developing in the absence of moisture-induced deformations (initial state). In addition, in the "center lift" mode, the sign of the peak moments changes, putting the top fiber in severe tension. With respect to mat loading, the increase in absolute peak moment from initial state to end of dry season is slightly smaller in the case of q=24kPa than that for 12kPa. This is most likely due to the partial suppression of the tendency for mid-term monotonic swelling under the mat center caused by a larger q.

The results for a strip mat show virtually the same trends as in the case of the circular mat. The only difference of practical interest is that the moments in the strip mat caused by the swelling/shrinkage of the foundation soil are slightly (less than 10%) smaller that those developing in the circular mat.

5 CONCLUSIONS

A simple constitutive model has been formulated and implemented in the finite element program Plaxis in order to perform numerical simulations of mat foundation – expansive soil interaction. The model is capable of predicting adequately both the swelling and collapse be-

havior of the soil as observed in oedometer testing. Coupled mechanical-unsaturated flow finite element analyses of a mat in medium to highly expansive marl with climatic input (rainfall/evaporation) consistent with the semi-arid climate of Nicosia show that the volume changes induced by moisture migration can cause a large increase in the mat bending moments, especially during the dry season. These extra moments should be taken into account in practice for the proper design of the mat reinforcement in order to avoid concrete damage. Analyses also show that the planar shape of the mat has only a small influence on the peak moments induced by soil swelling/shrinkage.

6 ACKNOWLEDGEMENTS

The authors are grateful to the personnel of the Technical Services of the University of Cyprus for their support in field work.

7 REFERENCES

Alonso, E.E., Vaunat, J., Gens, A. 1999. Modelling the mechanical behaviour of expansive clays. *Engineering Geology*, **54**(1), 173-183.

Constantinou, G., Petrides, G., Kyrou, K., Chrysostomou, C. 2002. *Swelling Clays: A Continuous Threat to the Built Environment of Cyprus*. UNOPS Project Final Report, Technical Chamber of Cyprus, Nicosia, Cyprus.

Galavi, V. 2010. *Groundwater flow, fully coupled flow deformation and undrained analyses in PLAXIS 2D and 3D*. Internal Report, Delft, Netherlands: PLAXIS bv Research Department.

van Genuchten, M.T. 1980. A closed-form equation for predicting the hydraulic conductivity of unsaturated soils. *Soil Science Society of America Journal*, **44**(5), 892-898.

Jahangir, E., Deck, O., Masrouri, F. 2013. An analytical model of soil–structure interaction with swelling soils during droughts. *Computers and Geotechnics*, **54**, 16-32.

Lazarou, G., Loukidis, D. Bardanis, M. 2019. Moisture migration under mat foundations in Nicosia marl. *Geotechnical and Geological Engineering*, **37**, 1585-1608.

Li, J. 1996. *Analysis and modelling of performance of footings on expansive soils*. PhD thesis, University of South Australia, Australia.

van der Merwe, D.H. 1975. Plasticity index and percentage clay fraction of soils. *Proceedings of the 4th Regional Conference in Africa on Soil Mechanics and Foundation Engineering*, Vol. 2, 166-167.

Mualem, Y. 1976. A new model for predicting the hydraulic conductivity of unsaturated porous media. *Water Resources Research*, **12**(3), 513-522.

Poulos, H.G. 1984. Parametric Solutions for Strip Footings on Swelling and Shrinking Soils. *Proceedings of the 5th International Conference on Expansive Soils*, Adelaide, Australia, pp. 149-153.

Vu, H.Q., Fredlund, D.G. 2004. The prediction of one-, two-, and three-dimensional heave in expansive soils. *Canadian Geotechnical Journal*, **41**(4), 713-737.

Walsh, P.F. 1974. *The design of residential slab-on-ground*, Technical Paper No. 5, CSIRO, Division of Building Research, Melbourne, Australia.

Williams, A.A.B., Donaldson, G. 1980. Building on Expansive Soils in South Africa: 1973-1980. *Proceedings of the 4th International Conference on Expansive Soils*, ASCE, Vol. 2, 834-844.

Wray, W.K. 1989. Field measurement of edge moisture variation distance. *Proceedings of the 12th International Conference on Soil Mechanics and Foundation Engineering*, Rio de Janeiro, Vol. 1, 663–666.